Agashe et al, Solar Energy Materials and Solar Cells, Volume 93, Issue 8, August 2009, Pages 1256-1262

Physical properties of highly oriented spray deposited fluorine doped tin dioxide films as transparent conductor

Chitra Agashe*[,1], J. Hüpkes[2], G. Schöpe[2] and M. Berginski[2]

[1]Solcoat Consultants, Flat 6, Dnyaneshwary Apartment, Plot 133/2, Prabha Society, Mayur Colony, Kothrud, PUNE -411038, **INDIA**.

[2]IEF-5 – Photovoltaik, Forschungszentrum Jülich GmbH, Jülich, D-52425, **GERMANY.**

***** corresponding author,

Tele. – 0091-20-25452472, Email: chitra_epf2003@yahoo.com,

Abstract

Heavily fluorine-doped tin dioxide films were deposited by spray pyrolysis using a high precursor concentration. The effect of film thickness was studied in the range 80-1230nm. The films were polycrystalline and preferentially oriented along [200]. The grain size, carrier mobility μ, carrier concentration N and resistivity reached ~230nm, 35 cm^2/Vs, $6x10^{20}$ cm^{-3} and $3x10^{-4}\Omega cm$, respectively, for 1000nm films. An unusual `direct and linear' μ-N dependence revealed the importance of the structural properties. The 1000nm thick films possessed an average visible transmittance ~81% and a reflectance ~66% at 2500nm. The electro-optical properties revealed their excellent quality as a TCO material.

Key words – tin dioxide films, spray pyrolysis, transparent conductor,

1. Introduction

Highly transparent and electrically conducting metal oxide based coatings (TCOs) are very interesting because of their wide variety of technological applications such as transparent contacts for solar energy conversion or optoelectronic devices, etc. [1-5]. Mainly investigated TCOs include thin films of cation / anion doped binary oxides like tin dioxide, indium oxide, zinc oxide. In addition, recent studies propose some ternary oxides and delafossite structures as competitive materials [6-8]. From an application's point of view, growing these films by a cost effective and simple technique such as spray pyrolysis is important. Spray pyrolysis is easily applicable to large-area deposition with the major advantage that the deposition can be performed at atmospheric conditions. Hence, developing transparent conductors by spray pyrolysis is of significance. Such an effort will assist one to enhance the commercial viability of the technique as also to obtain improved quality coatings.

Here we report a part of our work on development of opto-electronic device quality fluorine doped tin dioxide (SnO_2:F) films by spray pyrolysis technique. Our previous work on un-doped spray deposited SnO_2 films showed that precursor concentration is the most important process parameter controlling growth rate and structural properties, which thereby determine the electrical properties [9]. We had also seen that for differently doped SnO_2:F films, the rate of deposition will be decided by the competition between formation and etching of SnO_2 by HF, when a halo-acid like NH_4F is used as a source of fluorine [10]. Hence, to attain a reasonably high growth rate for SnO_2:F films, a high tin precursor concentration together with a heavy F doping was selected. An attempt was made to understand the growth and find the film thickness with optimized material properties.

2. Experimental

The spray pyrolysis technique was used to deposit SnO_2:F films. The precursor solution consisted of $SnCl_4.5H_2O$ dissolved in de-ionized water and methanol (volume ratio 1:9). The precursor concentration was 0.2M. NH_4F was added to maintain the F/Sn atomic ratio in the solution at 150 at.% [10]. The actual incorporation of fluorine into the film was expected to be very low due to the high volatility of fluorine compounds produced during the film deposition [11-12]. Corning 7059 glass was used as substrates. The

deposition temperature and solution flow rate were maintained at 450 (+/-5)°C and 1.5 ml/min, respectively. Other process parameters were kept constant as given earlier [13]. Films of thicknesses ~80nm, 250nm, 420nm, 640nm, 1000nm and 1230nm were deposited by spraying the solution of fixed composition in different amounts. The growth rate was ~ 25nm/min.

The film thickness was measured using a Talystep profilometer (roughness detector with a stylus - Taylor Hobson Model). Structural properties were investigated using a Philips PW 1840 diffractometer utilizing CuK_{α} (λ=1.542Å) radiation. The diffractograms for different spray deposited SnO_2:F films and the Asahi U film (thickness ~900nm) were taken under identical conditions. A comparison with JCPDS data [14] shows that the films were preferentially oriented along [200], accompanied by other orientations with very low intensities. The prominence of the [hkl] orientation was expressed in terms of a parameter `relative prominence (RP[hkl])' defined as,

RP[hkl] = (I[hkl]) / ∑(I[hkl]) (%) ---------------------------------- Equation (1)

where, I[hkl] is the relative intensity of [hkl] (peak height). The grain size and morphological features were derived from scanning electron microscopy [LEO (now Zeiss) field-emission SEM set-up]. Finer details of the film surface were analyzed using atomic force microscopy with a Nanoscope III - Digital Instruments. The physical properties of our films were compared with those of Asahi U SnO_2:F film which is a commercially available TCO substrate [15]. The electronic transport parameters of spray deposited SnO_2:F films and the Asahi U film were determined from room temperature Hall effect measurements done using a Keithley 926 Hall setup [16]. Transmittance and reflectance of the films were measured employing a Jasco-670 double beam spectrophotometer in a wavelength range 250–2500nm. Uncoated substrate was used as a reference for transmittance measurements. The optical gap was determined using a plot of the square of the absorption coefficient against the photon energy [17].

The measurement error for film thickness and Hall data was +/-5%. The optical data (T and R) may vary within +/-3%, possibly leading to an error in optical gap by ~0.1eV. The grain size varied within +/-10%.

3. Results and discussion

A: Structural properties – orientation and growth pattern

X-ray diffractograms of films with thickness 80nm, 250nm, 640nm, 1000nm and of the Asahi U film of thickness 900nm are shown in Fig. 1. Our films were highly oriented along [200]. Other orientations [110], [310], [301] and [400] were quite prominent, whereas [101] and [211] were very minor [14]. The Asahi U film was also oriented along [200]. Other orientations [110], [211], [310] and [301] were prevalent as compared to [101], [220], [321] and [400]. The film thickness dependence of I[200] (intensity of [200]) and RP[200] for our films is shown in Fig. 2a and that of RP[310], RP[301], RP[400] and RP[110] is shown in Fig. 2b. For the Asahi U film, the RP[hkl] values of prominent orientations were RP[200]=34.2, RP[110]=13.2, RP[211]=15.4, RP[310]=10.7 and RP[301]=13.7.

In the following an attempt is made to understand the occurrence of [200] with respect to 1) thin film growth / evolution of film structure with thickness, and 2) role of reactants as decomposition products of the precursor compounds in determining this growth. We then discuss the importance of a growth oriented along [200].

In the spray pyrolytic SnO_2 based deposition from hydrous $SnCl_4$, the impinging flux on the substrate undergoes an endothermic reaction. For deposition temperatures in the range of 350°C-500°C (in our case 450°C), the reactants' interaction with the substrate surface results in a heterogeneous type of nucleation in the very early stages of growth [18-19]. Hence, depending on the deposition conditions which define the non-equilibrium for film deposition, one may not observe an oriented type of growth in the first few layers. In our case, all films were mainly oriented along [200]. Very thin 80nm films showed a RP[110] of 30% which reduced with increasing thickness. This reduction in RP[110] was accompanied by the presence of [310], [301] and [400]. Due to this the prominence of [200] was less dominant for thinner films. The orientational effects further modified I[200] and RP[200] with thickness. From the JCPDS data for rutile SnO_2, [110] is the strongest reflex (100%) followed by [101] (80%), [211] (65%) and [200] (24%) [14]. The RP[hkl] for JCPDS data will also vary in the same way. Hence, the structural properties of a particular film can be compared with the JCPDS data by comparing the RP[hkl] variation for a film with the I[hkl] variation of the JCPDS data. But when one wants to compare the x-ray diffraction data for different

films one has to use normalized intensities like the relative prominence RP[hkl]. In the case of `textured thin films' of a material, a prominence of different orientations similar to JCPDS data cannot be expected. The prominent [200] growth can also arise from a higher growth rate consequent to more precursor concentration [9] which cannot be changed by even heavy fluorine doping [10]. A growth rate dependent evolution of the orientation has been discussed by Belanger et al. for chemical vapor deposited SnO_2 based films [20]. Our results indicate a presence of random growth (occurrence of [110]) for very thin films, which will be mostly nucleation controlled. When the thickness is increased by increasing both the amount of solution sprayed and the time of deposition (using constant solution flow rate), the effect of heterogeneous nucleation (and substrate surface) is reduced and the arrangement of growing crystallites gets gradually more defined by the preceding crystallites. As a result of the constraints developed by these preceding crystallites, the growth is expected to occur in a particular way, probably leading to a preferred growth. The occurrence of preferred growth and the growth direction depend on the material under study and the thermodynamics of deposition conditions. The orientation with minimum interfacial energy is favored. For tetragonal rutile SnO_2, [200] orientation has a low atomic density and a minimum interfacial energy [21-22]. Hence, the gradual increase of the prominence of [200] is anticipated. For thickness beyond a particular one (in our case 1μm), re-orientational effects may occur. This will be reflected in the form of enhanced intensities of other orientations. One can observe such a growth pattern when films were grown thick enough. This particular thickness obviously depends on other deposition conditions as well. Three stages of growth pattern including [200] oriented growth, were reported formerly also for spray pyrohydrolytic deposition, by Fujimoto et al. for SnO_2:Sb films [23] and by Miki-Yoshida et al. for un-doped SnO_2 films [24].

Other factors responsible in defining the preferred growth can be the stoichiometric and compositional changes, which occur during the growth itself. These will be governed mainly by the nature of the precursor, the impinging flux and the substrate temperature. Gordillo et al. observed that under comparable deposition conditions, the precursor with $SnCl_4$ leads to [200] oriented growth whereas preferential growth along [101], [211] and [301] was obtained by using $SnCl_2$ [25]. As discussed by Kaneko et al. such a preferred growth along [200] seems to arise from the O-Sn-O species forming at the

decomposition states of the source compound [26]. Fantini et al. discussed this issue for SnO_2 films grown by chemical vapor deposition and on the basis of structure factor calculations [27]. They observed that a significant concentration of oxygen vacancy as well as that of interstitially incorporated excess tin in the SnO_2 lattice will enhance the intensity of [200] and reduce the prominence of [110]. The influence of impinging flux (cationic and anionic species) in governing the growth rate and preferred growth was discussed by us in detail for un-doped SnO_2 films [9]. In the present case, the films were grown using a solution of high precursor concentration (0.2M) and hence, at considerably high rates (~25nm/min). Owing to this, the films are very likely to contain a large proportion of oxygen vacancies as well as excess tin, which will enhance the [200] growth. The interstitial incorporation of tin (Sn_i) is now well understood based on the recent work by Kılıç and Zunger [28]. It states that the energy of formation of Sn_i is lower than that for oxygen vacancy as well as the SnO_2:Sn_i is very stable due to the multivalency of Sn.

Both aspects discussed above support the preferred growth along [200].

Among many technological applications of SnO_2 based films, they are used as a transparent and conducting coating, with a typically required thickness between ~400nm and ~800nm. Our results show that in this range of thickness, when the films are grown with a precursor concentration of 0.2M, they are preferentially oriented along [200]. This orientation also is advantageous since it contains no Sn^{2+} trap states which would otherwise develop in the presence of oxygen vacancies and with the requirement of charge neutrality. Belanger et al. have investigated this aspect based on the stable multivalency of Sn [20] and have shown that there won't be any surface states as electron traps on the surface of crystallites grown along [200]. This implies that [200] oriented films will also have better electronic transport properties, which is of prime interest for any TCO application. In fact, as observed by Korotcenkov et al. such an oriented growth influenced the performance of SnO_2 film based gas sensor also [29]. Hence, it is quite important to understand the preferential growth in SnO_2 films, particularly along [200]. Figure 2 shows the contribution of thickness evolution to favor the growth along [200]. The contribution of the non-stoichiometry to define the preferred growth is through the growth rate as already discussed for spray deposited un-doped SnO_2 films [9]. Even a large variation of cation doping (antimony) could not affect the growth pattern for a wide range of precursor concentration (0.01M-0.2M) [30, 31]. The anion doping of F,

Cl and Br up to 120 at.% (in solution) also could not affect the preferred growth whereas its effect on the electro-optical properties was dependent on the electro-negativity and ionic size of the dopant [32, 33].

B: Morphological properties

The SEM pictures for these films and the Asahi U film [34] are shown in Fig. 3. The grain size increased with film thickness as seen from Fig. 4. Fig. 3a reveals that the films of ~250nm thickness showed the growth with crystallite faces pointing upwards. The tips look to be pyramidal and the growth gets densely populated for films of thickness ~420nm. The growth still has maintained the individuality of growing columns of [200], similar to the report by Omura et al. [35]. Figures 3(a-e) and 2(a-b), reveal that the films thinner than ~400nm consist of randomly oriented grains. In the thicker films, the [200] grains win the "growth race" and thus reduce the number of grains at the surface. The [200] grains grow from substrate to the surface and their lateral dimensions increase during growth unlike grains along other orientations. This is reflected by the elongated tips of the columns on the surface. This kind of morphology is maintained for thicker films along with an increase in grain size. The grain size derived from SEM characterization showed a gradual increase from ~70nm to ~230nm over the thickness range from ~80nm to ~1230nm (Fig. 4). The increased grain size for thicker films is a routinely observed and understood aspect of thin film TCO growth. To note, the morphological changes observed here are solely due to the change in thickness, since the preferred growth remained along [200] for the wide thickness range. On the contrary, Elangovan et al. observed a thickness dependent change in preferred orientation and consequent change in morphology for SnO_2:F films of thickness 840-1380nm, for the $SnCl_2.2H_2O/NH_4F$ precursor [36]. The primary role of precursor concentration in determining the growth rate which defines the growth pattern and preferred growth of un-doped SnO_2 films was established earlier [9]. In such films even a heavy F doping could not change the preferred growth [10]. In the present case the impinging flux of Sn and F was constant and the films of varied thickness were obtained by simply changing the amount and time of deposition. Hence, the morphological changes directly follow the thickness evolution.

The AFM investigations were consistent with the SEM studies. The surface roughness increased with film thickness as shown in Fig. 4 and seems to saturate for thicker films above 1000nm. The change in

pyramidal topography was anticipated based on our discussion of structural properties using x-ray diffraction and SEM. The rms roughness of Asahi U film of comparable thickness is higher though the grains are even larger. The multi-orientational nature of the Asahi U films (see Fig. 1) may also contribute to the higher rms roughness.

The importance of rough surface of SnO_2:F TCO in the light trapping effect of amorphous silicon based solar cells was discussed in depth by Gordon et al. [37]. Recently, Kambe et al. investigated the effect of surface topography on the light-trapping effect of microcrystalline silicon thin film solar cells [38]. Among the flat, pyramidal and rectangular surface topography studied by them, the pyramidal one proved to be the best. Haase and Stiebig conducted detailed theoretical investigations to obtain an optimum light trapping scheme in amorphous as well as microcrystalline silicon based thin film solar cells [39-40]. Their results also reveal a necessity of three dimensional pyramidal interface with front TCO.

The height distribution for all SnO_2:F films and Asahi U film was standard Gaussian in nature. The surface structure is composed of sine waves with different spatial wavelengths. Their contributions can be obtained through the power spectral density function (PSD) as Fourier transformation of the real surface from AFM data. Kluth et al. studied PSD functions of different surface topographies [41]. Figure 5 shows the PSD analysis for spray deposited films and the Asahi U film. In the range of low spatial wavelengths (up to 100nm), an increase in the PSD with film thickness could not be seen prominently. On the contrary, for larger spatial wavelengths PSD increases with film thickness and the saturation shifts to larger wavelength. This behavior reflects the lateral size of the grains, as larger grains cause contributions of larger wavelengths. The PSD of thick sprayed films corresponds well with the Asahi U type SnO_2:F. However, there is still a scope for improvement of surface structure regarding size and thickness dependence.

C: Electrical properties – resistivity, carrier concentration and mobility

The Hall resistivity, carrier concentration and mobility are plotted in Fig. 6 as a function of film thickness. The resistivity drops by a factor of ~13, from about $4\times10^{-3}\Omega$cm to $2.8\times10^{-4}\Omega$cm, when the thickness is increased from 80nm to 1230nm.

The carrier concentration is above $1x10^{20}cm^{-3}$ and increases with film thickness (Fig. 6a). Such a high carrier concentration can arise from any one or all of the following factors, viz. 1) presence of oxygen vacancies, 2) Sn incorporation at interstitial sites, 3) incorporation of dopant fluorine and 4) inclusion of residual chlorine through the precursor. In the spray deposited SnO_2 films, the oxygen vacancies are present since the growth takes place in a chemically reducing surrounding (the precursor contains alcohol) [10]. Due to a high precursor concentration, the expected Sn incorporation at interstitial sites will provide conduction electrons consequent to an overlap of outer orbitals when they can easily occupy the most spacious combination of interstitial lattice sites (1/2, 0, 1/2) and (0, 1/2, 1/2) [9, 28]. Our recent work on thickness evolution of un-doped SnO_2 films with a wide range of precursor concentration (0.01M-0.4M), suggests that with 0.2M concentration, the interstitial Sn becomes more dominant than oxygen vacancies in assigning a high carrier concentration [42]. The F incorporation into the growing film was kept constant through the impinging flux. It seems that when the fluorine doping is changed, at lower dopant levels it first tries to reduce the lattice strain otherwise present with the oxygen vacancies by occupying the vacancy sites. This is followed by the gradual incorporation at regular oxygen sites. The doping level `150 at.% in solution' was observed to be such a moderately high level that F occupies the oxygen sites. This was observed before from the reduced prominence of RP[200] [10, 27]. To note, F incorporation at oxygen sites increases the carrier concentration unlike the F occupying the oxygen vacancies. Hence, this doping level will increase the carrier concentration. The inclusion of Cl will depend on the temperature of the growing surface. Our previous work on un-doped SnO_2 films shows that under similar experimental conditions, Cl inclusion is below the detection limit [9]. Hence, the high carrier concentration owes to 1) the oxygen vacancies, 2) the interstitially incorporated Sn and 3) fluorine incorporation at regular oxygen sites.

During the growth of these films, the impinging flux of Sn, O and F is kept constant due to the fixed deposition conditions. The influence of the heated substrate and the growth induced effects will govern the electrical properties through the consequent changes in the structural and compositional properties. The role of the substrate surface and the thickness up to which the substrate surface can affect the film growth is the same for thin and thick films. Obviously, when the growth is continued to make a film of

thickness beyond a particular one, the previously grown layers of the crystallites are expected to affect the structure and composition of the growing layers. The structure of the lower layers constrains the arrangement of impinging species and the interaction processes between them determine the composition of the growing crystallites. Also, the substrate-film interface has a stronger influence in assigning the material properties of very thin films. We expect then the transport parameters to improve with film thickness, which can be seen more directly when the growth pattern is maintained, like here along [200]. As revealed by Fantini et. al [27], the enhanced growth along [200] is also associated with the increased incorporation of interstitial Sn, oxygen vacancy and F inclusion at oxygen sites, which will contribute to increase the carrier concentration. The thickness dependence of carrier concentration and carrier mobility should be seen in this context.

The carrier mobility (Fig. 6b) improves linearly with film thickness which is consistent with the enhancement of preferred growth along [200] as well as the increase in grain size with film thickness, as shown in Figs. 2a and 4, respectively. The grain size dependence of carrier mobility is explicit from Fig. 7. Our results are particularly encouraging since the linear thickness dependence of mobility is maintained up to the film thickness ~1000nm when the mobility reaches ~36cm^2/Vs. This is comparable to the mobility of Asahi U films, even though our films have a grain size smaller than that of Asahi U (see Fig. 4). This clearly shows the advantage of a preferred growth along [200]. The columnar growth anticipated for [200] [35] giving a compact structure for thicker films (see the section on SEM above) will also assist in increasing the mobility.

Figure 8 reveals a linear increase in carrier mobility with the carrier concentration for films under study. This is very interesting and also unusual, since a typical μ-N relation for TCOs shows a different behavior with such a high N [43-46]. Our results show that the μ and N are basically limited by the structural properties, viz. [200] prominence and grain size, and can be improved by film thickness. This implies that high quality films can be achieved by a careful control of film structure. To point out, these results would perhaps propose a new approach to the present thinking of transport in heavily doped TCOs.

D: Optical properties

Figure 9 shows the transmittance and reflectance of the 420nm, 640nm and 1000nm thick spray deposited SnO_2:F films. The films show a high transmittance in the visible spectral range and increasing reflectance in the near infrared range. Typically for 640nm film, the average visible transmittance, near infrared reflectance, plasma wavelength (determined from the absorption peak) and optical gap are ~84% (for 0.55-0.85μm), 66% (for 2.5μm), 1.5μm and 4.4eV, respectively. The optical gap is higher than that for un-doped SnO_2 films 3.78 eV [47]. This is consistent with the Moss-Burstein widening for fluorine doped SnO_2 films [48]. The transition from highly transparent in the visible region to highly reflecting in the near infrared region looks quite sharp. This sharpness owes to the high carrier mobility for the high carrier concentration.

4. Conclusions

Spray deposited transparent conducting SnO_2:F films were investigated in detail in dependence of film thickness which was varied through the deposition duration. Films of thicknesses between 80-1230nm showed a preferred growth along [200] which dominated the electrical transport properties. The minimum resistivity $3x10^{-4}$Ωcm is close to the lowest reported for spray deposited SnO_2:F films and is controlled by the linear increment in the carrier concentration and mobility with the film thickness. The morphological features show a pyramidal topography in spray deposited films comparable to the morphology of the Asahi U film. The spray deposited films of thickness comparable to that of Asahi U film also possess competitive electrical and morphological properties, proposing them as a high quality transparent conductor.

Acknowledgments

The authors thank A. Doumit (IEF-5-Photovoltaik, FZJ, Germany) for extensive technical assistance.

References

[1] B. Rech, O. Kluth, T. Repmann, T. Roschek, J. Springer, J. Müller, F. Finger, H. Stiebig and H. Wagner, Solar Energy Mater. and Solar Cells 74 (2002) 439-447.

[2] T. Kamiya and H. Hosono, Int. J. Appl. Ceram. Technol. 2 (2005) 285-294.

[3] T. Minami, Semicond. Sci. Technol. 20 (2005) S35-S44.

[4] P. Veluchamy, M. Tsuji, T. Nishio, T. Aramoto, H. Higuchi, S. Kumazawa, S. Shibutani, J. Nakajima, T. Arita, H. Ohyama, A. Hanafusa, T. Hibino and K. Amura, Solar Energy Mater. and Solar Cells 67 (2001) 179-185.

[5] K. L. Chopra, S. Major and D. K. Pandya, Thin Solid Films 102 (1983) 1-46.

[6] O. Kluth, C. Agashe, J. Hüpkes, J. Müller and B. Rech Proceeding - 3rd World Conference on Photovoltaic Energy Conversion, May 11-18, 2003, Osaka, Japan, 2 (2003) 1800-1803.

[7] D. Ko, K. Poeppelmeier, D. Kammler, G. Gonzalez, T. Mason, D. Williamson, D. Young and T. Coutts, J. Solid State Chemistry 163 (2002) 259-266.

[8] M. Marquardt, N. Ashmore and D. Cann, Thin Solid Films 496 (2006) 146-156.

[9] C. Agashe, M. Takwale, V. Bhide, S. Mahamuni and S. Kulkarni, J. Appl. Phys. 70 (1991) 7382-7386.

[10] C. Agashe and S. Major, J. Mater. Sci. 31 (1996) 2965-2969.

[11] E. Shanthi, A. Banerjee, V. Dutta and K. L. Chopra, J. Appl. Phys. 53 (1982) 1615-1621.

[12] J. C. Manifacier, Thin Solid Films 90 (1982) 297-308.

[13] C. Agashe, M. Takwale, B. Marathe and V. Bhide, Sol. Energy Mater. 17 (1988) 99-117.

[14] Joint Committee on Powder Diffraction Standards - Powder Diffraction File, International Center for Diffraction Data, Swarthmore, PA, 1988, Card No. 21-1250.

[15] K. Sato, Y. Gotoh, Y. Wakayama, Y. Hayashi, K. Adachi and H. Nishimura, Reports Res. Lab. Asahi Glass Co. Ltd., 42 (1992) 129-137.

[16] W. R. Runyan Semiconductor Measurements and Instrumentation (McGraw Hill, Kogakusha Ltd., Tokyo, 1975) p. 137.

[17] V. Srikant and D. R. Clarke, J. Appl. Phys. 83 (1998) 5447-5451.

[18] V. Vasu and A. Subrahmanyam, Thin Solid Films 189 (1990) 217-225.

[19] V. Vasu and A. Subrahmanyam, Thin Solid Films 193/194 (1990) 973-980.

[20] D. Belanger, J. P. Dodelet, B. A. Lombos and J. I. Dickson, J. Electrochem. Soc. 132 (1985) 1398-1405.

[21] M. Fantini, I. Torriani and C. Constantino, J. Cryst. Growth 74 (1986) 439-442.

[22] J. M. Poate, K. N. Tu and J. W. Mayer, Thin Films Inter-diffusion and Reactions (Eds. J.M. Poate and J. W. Mayer, Wiley, New York, 1978)

[23] M. Fujimoto, Y. Nishi, A. Ito, T. Mishuku, H. Uda and S. Shirasaki, Jpn. J. Appl. Phys. 27 (1988) 534-539.

[24] M. Miki-Yoshida and E. Andrade, Thin Solid Films 224 (1993) 87-96.

[25] G. Gordillo, L. C. Moreno, W. de la Cruz and P. Teheran, Thin Solid Films 252 (1994) 61-66.

[26] S. Kaneko, I. Yagi, K. Murakami and M. Okuya, Solid State Ionics 141–142 (2001) 463-470.

[27] M. Fantini and I. Toriani, Thin Solid Films 138 (1986) 255-265.

[28] Ç. Kılıç and A. Zunger, Phys. Rev. Lett. 88 (2002) 95501:1-95501:4.

[29] G. Korotcenkov, M. DiBattista, J. Schwank and V. Brinzari, Mater. Sci. and Engg. B77 (2000) 33-39.

[30] D. Goyal, C. Agashe, M. Takwale and V. Bhide, J. Cryst. Growth 130 (1993) 567-570.

[31] D. Goyal, C. Agashe, M. Takwale and V. Bhide, J. Appl. Phys., 73 (1993) 7520-7523.

[32] C. Agashe and S. Major, J. Phys. D - Appl. Phys. 29 (1996) 2988-2991.

[33] C. Agashe and S. Major, J. Mater. Sci. Lett. 15 (1996) 497-499.

[34] J. Müller, G. Schöpe, B. Rech, H. Schade, P. Lechner, R. Geyer, H. Stiebig and W. Reetz, Proceeding - 3rd WCPEC, May 11-18, 2003, Osaka, Japan, 1 (2003) 503-506.

[35] K. Omura, P. Veluchamy, M. Tsuji, T. Nishio and M. Murozono, J. Electrochem. Soc. 146 (1999) 2113-2116.

[36] E. Elangovan and K. Ramamurthi, Appl. Surf. Sci. 249 (2005) 183-196.

[37] R. G. Gordon, J. Proscia, F. Ellis and A. E. Delahoy, Solar Energy Mater. 18 (1989) 263-281.

[38] M. Kambe, M. Fukawa, N. Taneda, Y. Yoshikawa, K. Sato, K. Ohki, S. Hiza, A. Yamada and M. Konagai, Proceeding - 3rd World Conference on Photovoltaic Energy Conversion, May 11-18, 2003, Osaka, Japan, 2 (2003) 1812-1815.

[39] C. Haase and H. Stiebig, Proceeding - 21st European Photovoltaic Solar Energy Conf., Sept. 4-8, 2006, Dresden, Germany, 2 (2006) 1712-1715.

[40] C. Haase and H. Stiebig, Prog. in Photovoltaics: Res. Appl. 14 (2006) 629-641.

[41] O. Kluth, C. Zahren, H. Stiebig, B. Rech and H. Schade, 19th European Photovoltaic Solar Energy Conference, 7-11 June 2004, Paris, France, 2 (2004) 1587-1590.

[42] C. Agashe, J. Hüpkes, A. Doumit and M. Berginski, thickness evolution in un-doped SnO_2 films, in preparation.

[43] J. R. Bellingham, W. A. Phillips and C. J. Adkins, J. Mater. Sci. Lett. 11 (1992) 263-265.

[44] K. Ellmer, J. Phys. D - Appl. Phys. 34 (2001) 3097-3108.

[45] T. Pisarkiewicz, K. Zakrzewska and E. Leja, Thin Solid Films 174 (1989) 217-223.

[46] T. Minami, MRS Bull., 25 (2000) 38-44.

[47] A. L. Dawar, A. Kumar, S. Sharma, K. N. Tripathi, P. C. Mathur, J. Mater. Sci., 28 (1993) 639-644.

[48] E. Burstein, Phys. Rev., 93 (1954) 632-633.

Figure Captions

Figure 1 : X-ray diffractograms of spray deposited SnO_2:F films with thickness; a) 80nm, b) 250nm, c) 640nm, d) 1000nm. Also shown is (e) that of Asahi U film - 900nm thick.

Figure 2 : Thickness dependence of a) I[200], RP[200] and b) RP[hkl] for spray deposited SnO_2:F films.

Figure 3 : SEM pictures of film surface for a) 250nm, b) 420nm, c) 640nm, d) 1000nm and e) 1230nm spray deposited SnO_2:F films. Also shown in f) is an SEM micrograph for 900nm Asahi U film. All pictures were taken at the same magnification and viewing angle.

Figure 4 : Film thickness dependence of grain size (SEM) and RMS roughness (AFM) for spray deposited SnO_2:F films. The grain size and RMS roughness for Asahi U film were ~250 nm and ~43nm respectively.

Figure 5 : Power spectral density as a function of wavelength for the SnO_2:F films of different thickness – a) 420nm, b) 640nm, c) 1000nm and d) 1230nm and for Asahi U film.

Figure 6 : Film thickness dependence of resistivity (ρ), carrier concentration (N) and mobility (μ) for spray deposited SnO_2:F films. The respective parameters for 900nm Asahi U film were $8.8 \times 10^{-4}\Omega cm$, $2.2 \times 10^{20} cm^{-3}$ and $32.4 cm^2/Vs$.

Figure 7 : Grain size dependence of carrier mobility for spray deposited SnO_2:F films.

Figure 8 : Linear dependence of μ on N for spray deposited SnO_2:F films. Also shown for comparison is the μ-N data for spray deposited un-doped SnO_2 film (our work in progress) and Asahi U film.

Figure 9 : Transmittance and reflectance of spray deposited SnO_2:F films.

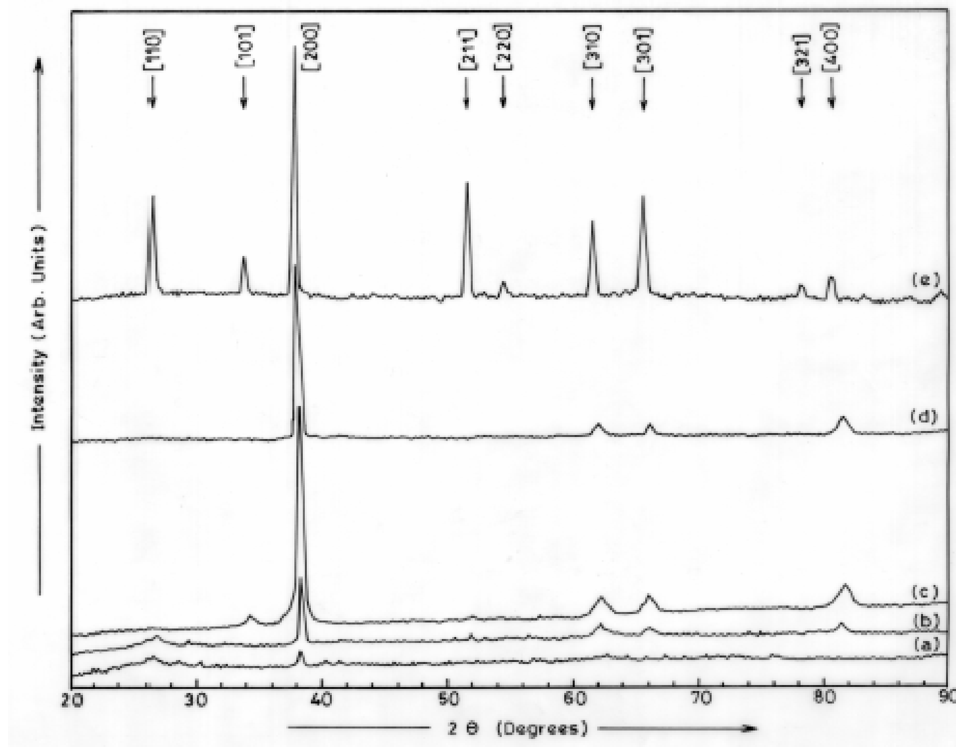

Figure 1: X-ray diffractograms of spray deposited SnO_2:F films with thickness; a) 80nm, b) 250nm, c) 640nm, d) 1000nm. Also shown is (e) that of Asahi U film – 900nm thick.

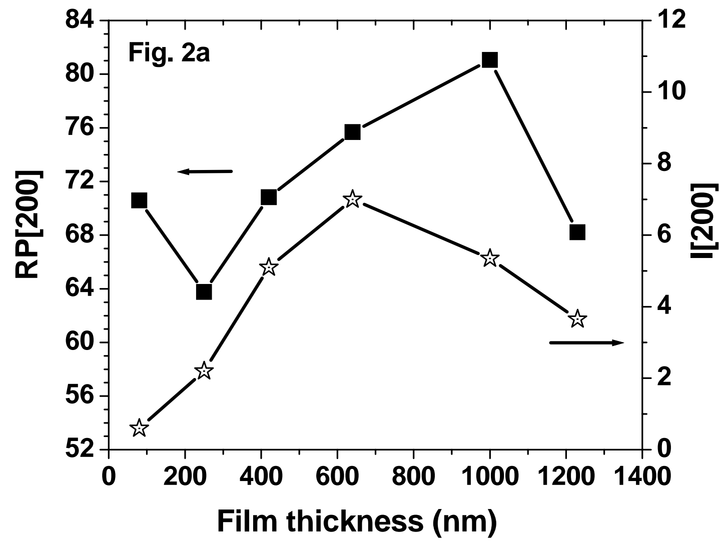

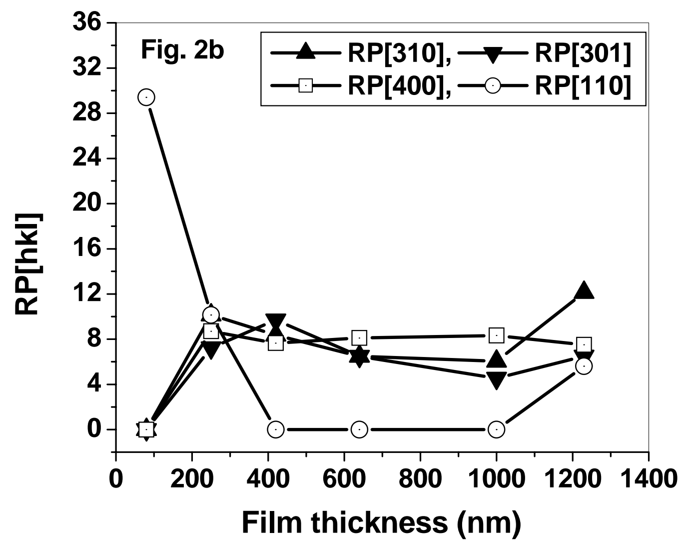

Figure 2 : Thickness dependence of a) I[200], RP[200] and b) RP[hkl] for spray deposited SnO_2:F films.

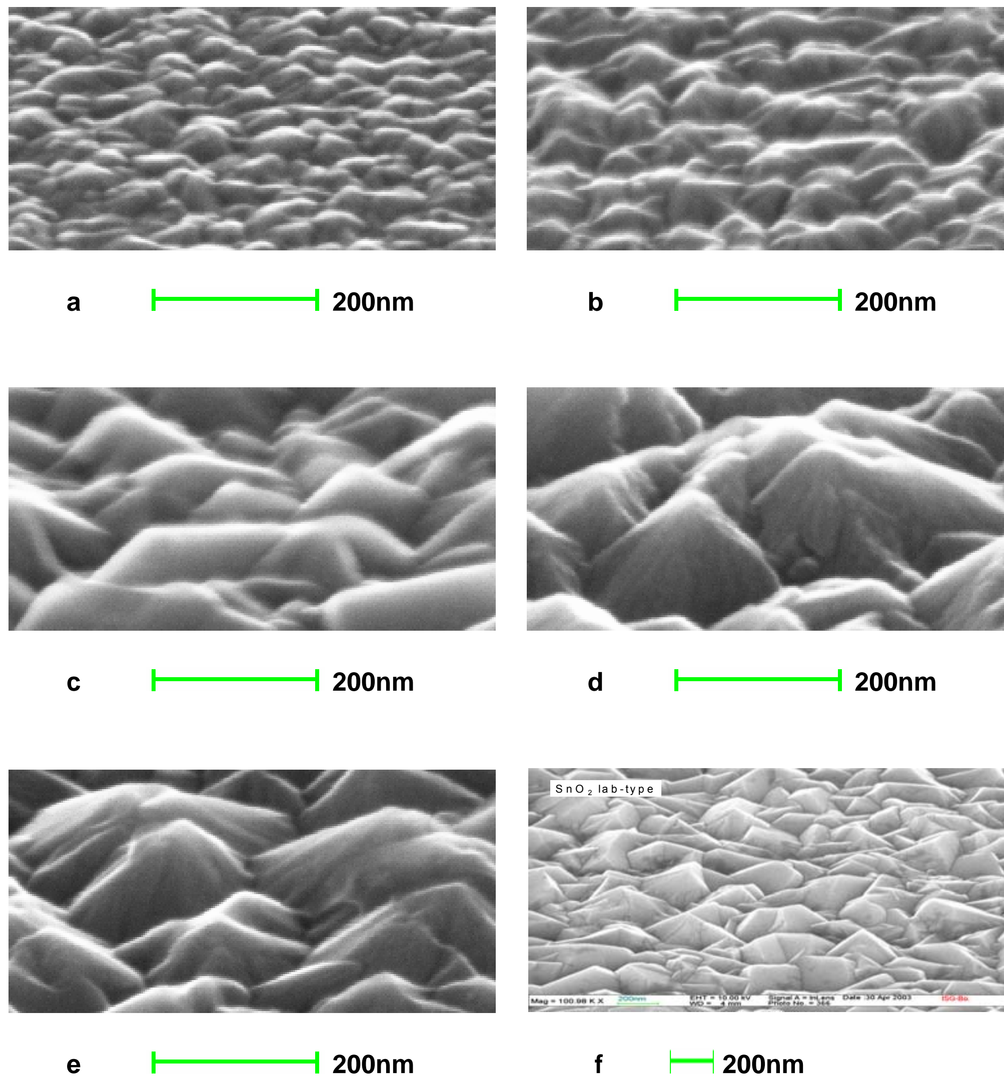

Figure 3 : SEM pictures of film surface for a) 250nm, b) 420nm, c) 640nm, d) 1000nm and e) 1230nm spray deposited SnO_2:F films. Also shown in f) is an SEM micrograph for 900nm Asahi U film. All pictures were taken at the same magnification and viewing angle.

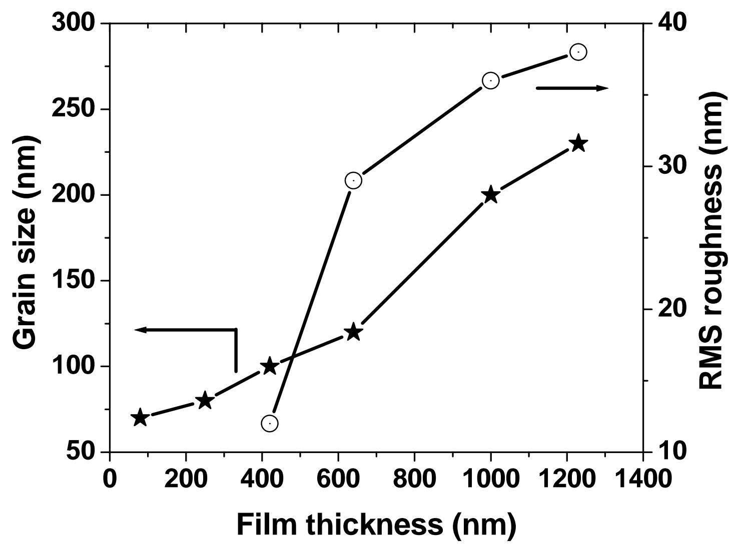

Figure 4 : Film thickness dependence of grain size (SEM) and RMS roughness (AFM) for spray deposited SnO_2:F films. The grain size and RMS roughness for Asahi U film were ~250 nm and ~43nm respectively.

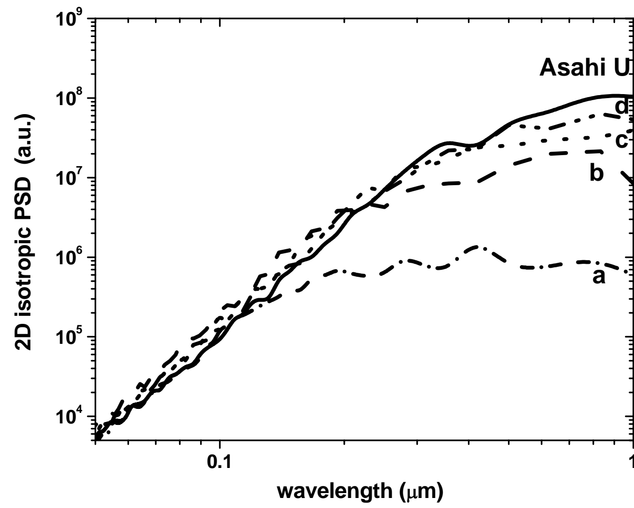

Figure 5: Power spectral density as a function of wavelength for the SnO_2:F films of different thickness – a) 420nm, b) 640nm, c) 1000nm and d) 1230nm and for Asahi U film.

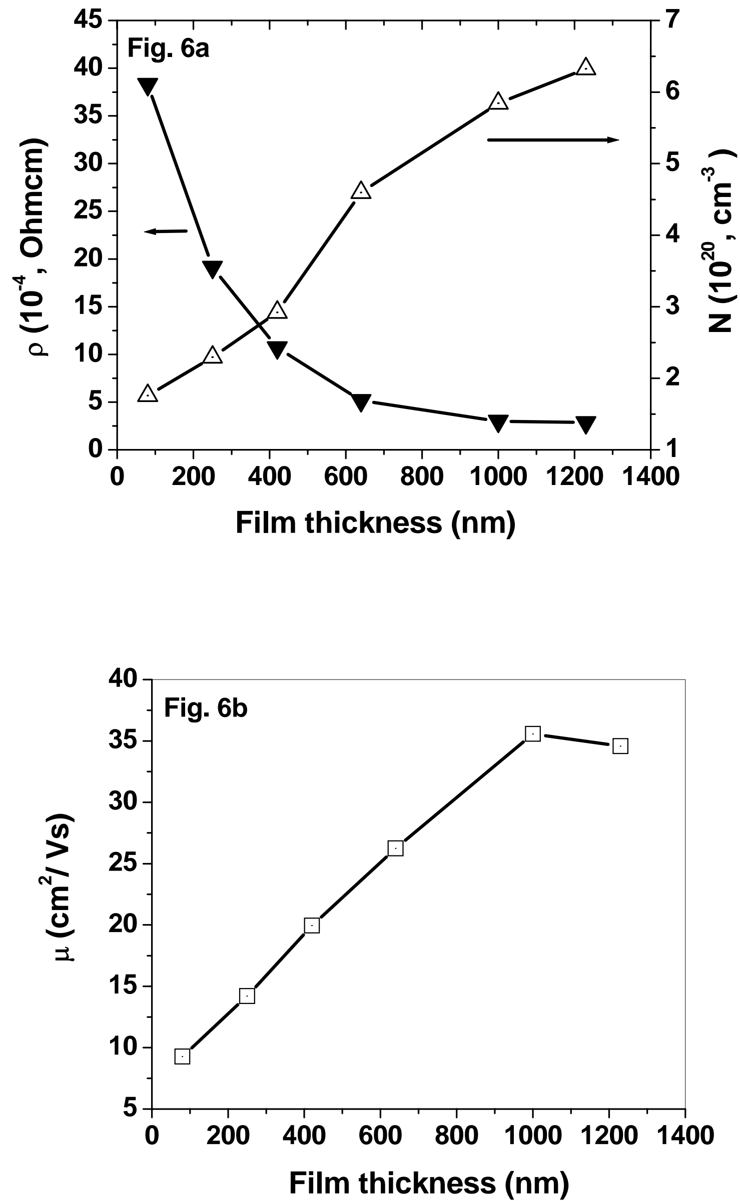

Figure 6 : Film thickness dependence of resistivity (ρ), carrier concentration (N) and mobility (μ) for spray deposited SnO_2:F films. The respective parameters for 900nm Asahi U film were 8.8×10^{-4}Ωcm, 2.2×10^{20}cm^{-3} and 32.4cm^2/Vs.

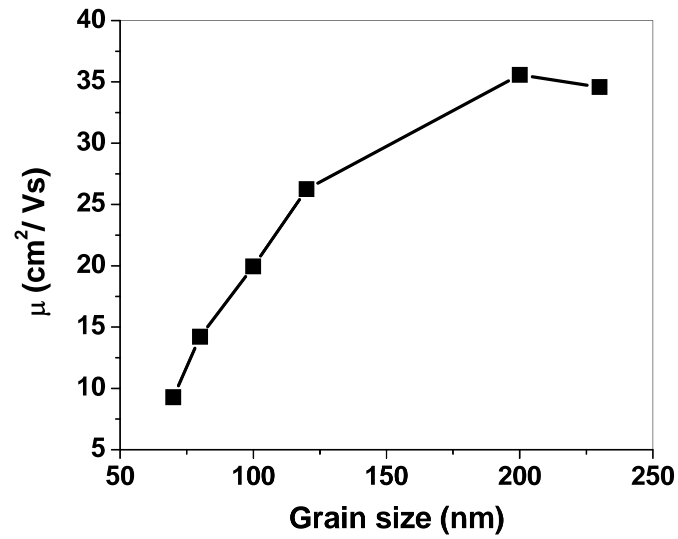

Figure 7 : Grain size dependence of carrier mobility for spray deposited SnO_2:F films.

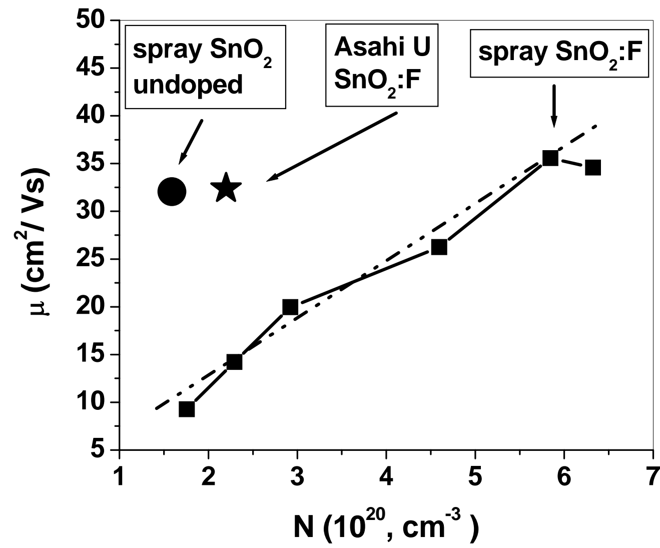

Figure 8 : Linear dependence of μ on N for spray deposited SnO_2:F films. Also shown for comparison is the μ-N data for spray deposited un-doped SnO_2 film (our work in progress) and Asahi U film.

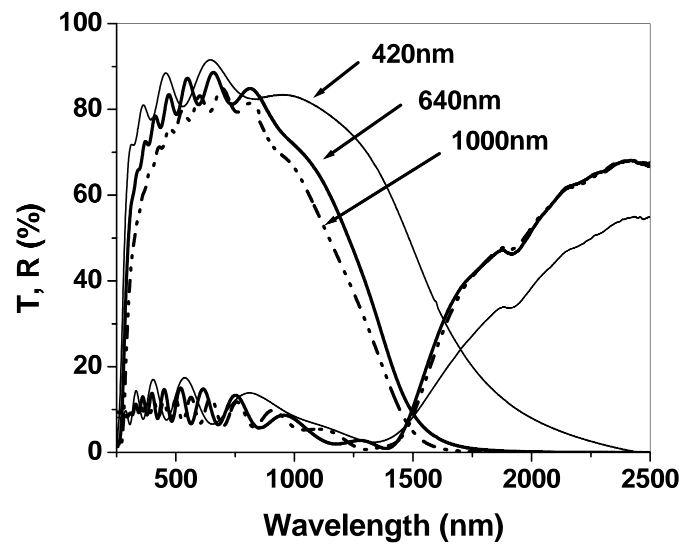

Figure 9 : Transmittance and reflectance of spray deposited SnO_2:F films.